Quality-Controlled Upper-Air Sounding Dataset for TiMREX/SoWMEX: Development and Corrections

PAUL E. CIESIELSKI,* WEN-MING CHANG,+ SHAO-CHIN HUANG,# RICHARD H. JOHNSON,* BEN JONG-DAO JOU,+ WEN-CHAU LEE,@ PO-HSIUNG LIN,+ CHING-HWANG LIU,# AND JUNHONG WANG@

* *Department of Atmospheric Science, Colorado State University, Fort Collins, Colorado*
+ *Department of Atmospheric Sciences, National Taiwan University, Taipei, Taiwan*
# *Department of Atmospheric Sciences, Chinese Cultural University, Taipei, Taiwan*
@ *National Center for Atmospheric Research,& Boulder, Colorado*

(Manuscript received 13 April 2010, in final form 27 July 2010)

ABSTRACT

During the Terrain-Influenced Monsoon Rainfall Experiment (TiMREX), which coincided with Taiwan's Southwesterly Monsoon Experiment—2008 (SoWMEX-08), the upper-air sounding network over the Taiwan region was enhanced by increasing the radiosonde (''sonde'') frequency at its operational sites and by adding several additional sites (three that were land based and two that were ship based) and aircraft dropsondes. During the special observing period of TiMREX (from 15 May to 25 June 2008), 2330 radiosonde observations were successfully taken from the enhanced network. Part of the challenge of processing the data from the 13 upsonde sites is that four different sonde types (Vaisala RS80, Vaisala RS92, Meisei, and Graw) were used. Post–field phase analyses of the sonde data revealed a significant dry bias in many of the sondes—in particular, in the data from the Vaisala RS80 sondes that were used at four sites. In addition, contamination of the sonde data by the ship's structure resulted in poor-quality low-level thermodynamic data at a key oceanic site. This article examines the methods used to quality control the sonde data and, when possible, to correct them. Particular attention is given to the correction of the humidity field and its impact on various convective measures. Comparison of the corrected sonde humidity data with independent estimates shows good agreement, suggesting that the corrections were effective in removing many of the sonde humidity errors. Examining various measures of convection shows that use of the humidity-corrected sondes gives a much different perspective on the characteristics of convection during TiMREX. For example, at the RS80 sites, use of the corrected humidity data increases the mean CAPE by ~500 J kg^{-1}, decreases mean convective inhibition (CIN) by 80 J kg^{-1}, and increases the midlevel convective mass flux by greater than 70%. Ultimately, these corrections will provide more accurate moisture fields for diagnostic analyses and modeling studies.

1. Introduction

The Terrain-Influenced Monsoon Rainfall Experiment (TiMREX) was a joint U.S.–Taiwan multiagency field program conducted in May and June of 2008 that coincided with Taiwan's Southwesterly Monsoon Experiment—2008 (SoWMEX-08). The overarching objectives of these experiments are to improve understanding of the physical processes associated with the terrain-influenced heavy precipitation systems and the monsoon environment in which they are embedded and, ultimately, to better forecast heavy rain–producing convective systems, which can cause substantial property damage and impede agricultural production. Details of the experiment's design, motivation, and goals are summarized in Jou and Lee (2009). The focus of these experiments is on the mei-yu season when strong, moist low-level southwesterly flow develops over the northern South China Sea associated with the onset of the east-Asian summer monsoon (Chen 2004).

To accomplish the experimental goals, intensive field observations were conducted during the 15 May–25 June

& The National Center for Atmospheric Research is sponsored by the National Science Foundation.

Corresponding author address: Paul E. Ciesielski, Dept. of Atmospheric Science, Colorado State University, Fort Collins, CO 80523.
E-mail: paulc@atmos.colostate.edu

DOI: 10.1175/2010JTECHA1481.1

2008 period. Many of these observations were concentrated on the southern end of Taiwan and its upstream environment, providing an unprecedented spatial and temporal resolution of the flow associated with precipitation systems. In addition to an enhanced sounding network over this region, a large suite of instruments was deployed during this period, including several radars (two of which had polarimetric capabilities), a 915-MHz wind profiler, numerous rain gauges, surface observations, and several ground-based GPS systems for monitoring moisture conditions. Measuring the atmospheric state with these multiple platforms allows for rigorous cross calibration that can greatly enhance the accuracy of the data, which is crucial for post–field phase diagnostic, data assimilation, and numerical modeling studies.

Considering the numerous applications of upper-air radiosondes (''sondes''), several efforts in recent years have been undertaken to create high-fidelity field-program sounding datasets. Most issues in correcting these datasets are related to sonde moisture biases (Wang et al. 2002; Nakamura et al. 2004; Ciesielski et al. 2003; Nuret et al. 2008; Yoneyama et al. 2008; Ciesielski et al. 2009). Correcting sonde humidity has resulted in improved diagnostic analyses of convection, atmospheric budgets, and the diurnal cycle (Guichard et al. 2000; Ciesielski et al. 2009); better simulations of convection and improvements in NWP (Lorenc et al. 1996; A. Agusti-Panareda et al. 2010); and datasets that are better suited for model validation.

During TiMREX, the upper-air sounding network over and upstream of Taiwan was enhanced by increasing the sonde frequency at several of the operational sites and by adding five sounding sites. Two of these additional sites were on research vessels to the north and southwest of Taiwan. To improve sampling of the large-scale environment to the south of Taiwan, the TiMREX project office provided sondes to the Philippines to increase the launch frequency at Laoag on the northwest coast of Luzon. In addition, 16 dropsonde missions were conducted over oceans, primarily to document the kinematic and thermodynamic structures of the low-level jet upstream of Taiwan. Part of the challenge of processing the data from the 13 upsonde sites is that four different sonde types (Vaisala RS80A, Vaisala RS92, Meisei, and Graw) were used. Analysis of the sonde data shows that a substantial dry bias was present in many of the sondes.

The purpose of this paper is to document the quality-control (QC) procedures and corrections that were applied to the TiMREX sonde dataset and to examine the impact of the corrections. In section 2, details of the upper-air network deployed in TiMREX are described, as well as the stages involved in the QC process. The humidity biases at the various sites are examined in section 3, and section 4 describes the details of their correction. Section 5 is devoted to evaluating the corrections. Upstream soundings from the southern ship represent a key source of observations in TiMREX; however, examination of these data reveals that the low-level thermodynamic fields were contaminated by the ship structure. Section 6 describes a procedure to correct the contaminated data points. Impacts of the corrections on various moisture-related analyses are presented in section 7, and results are summarized in section 8.

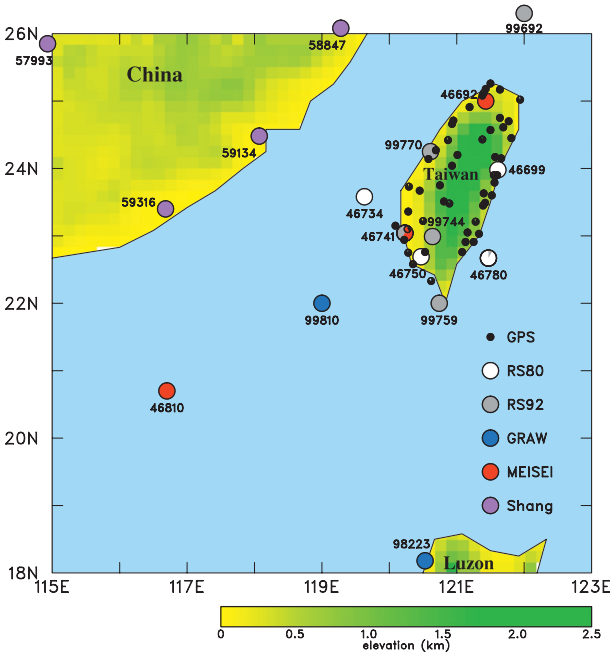

FIG. 1. Sounding network for TiMREX with location of sounding sites and type of sounding system indicated with color-coded circles. Table 1 lists the station numbers with their corresponding names. Sounding sites in China are not part of the enhanced sonde network for TiMREX. The GPS network over Taiwan is denoted with black filled circles.

2. Upper-air network and QC process

a. TiMREX sonde network

The enhanced sonde network of TiMREX consisted of 13 sites with upsonde observations in Taiwan and its vicinity: a combination of eight operational stations and five supplementary sites specifically deployed for the field experiment. These sites, along with a few of the operational stations in mainland China, are shown in Fig. 1, in which the sonde type used at each site is indicated. Table 1 summarizes the relevant aspects of each sounding site. As noted in this table and in Fig. 1, four of

TABLE 1. Summary of pertinent station information for sounding sites in TiMREX. Site identifiers (ID) and station names listed in boldface indicate operational sites with established sounding facilities. MEISEI denotes the use of Meisei RS80 sondes, and RS indicates the use of Vaisala sondes; tracking of the balloon to measure winds was done with either ATR or GPS. Vertical resolution listed is the native resolution in the datasets for levels 1–3; No. refers to the number of successful sonde launches during TiMREX SOP. CDF refers to the CDF matching method, VCC to use of Vaisala-corrected coefficients, YON to Yoneyama daytime correction, and CP08 to Cady-Pereira daytime correction.

Site ID	Station name	System type	Launch frequency (sondes per day): SOP, IOP, EOP	Vertical resolution (s)	No.	Dates of operation	Corrections applied
46692	**Banchiao**	MEISEI–ATR	4, 4, 8	5	184	16 May–25 Jun	CDF, YON
46699	**Hualien**	RS80–ATR	4, 4, 8	2	185	15 May–25 Jun	CDF, CP08
46734	**Makung**	RS80–ATR	4, 8, 8	2	232	15 May–26 Jun	VCC, CP08
46741	**Tainan**	MEISEI–ATR	4, 4, 8	5	76	27 May–6 Jun	CDF, YON
		RS92–GPS	4, 4, —	1	53	12–23 Jun	YON
46750	**Pingdong**	RS80–ATR	5, 8, 8	2	248	15 May–26 Jun	VCC, CP08
		RS92–ATR	—, 4, —	”	18	3 Jun–10 Jun	YON
46780	**Green Island**	RS80–ATR	4, 4–8, 8	2	201	16 May–21 Jun	VCC, CP08
		RS92–GPS	4, 4–8, —	”	18	22–26 Jun	YON
46810	**Dongsha Island**	MEISEI–ATR	4, 4, 4	5	156	7 May–25 Jun	CDF, YON
		RS92–ATR	1, —, —	2	1	10 Jun	YON
98223	**Laoag, Philippines**	Graw–GPS	2, 2, 2	10	67	15 May–30 Jun	CDF, YON
99692	Ship *N*	RS92–GPS	4, 4, 4	2	46	30 May–10 Jun	YON
99744	Liou-Guei	RS92–GPS	4, 4–8, 8	1	218	14 May–26 Jun	YON
99759	Henchun	RS92–GPS	4, 4, 8	1	140	14 May–26 Jun	YON
99770	Taichung	RS92–GPS	4, 8, 8	2	163	15 May–17 Jun	YON
99810	Ship *S*	Graw–GPS	4, 4, 4	1	134	14 May–21 Jun	Low-level T, T_d
	Dropsondes	RS92–GPS	Variable	0.5	190	2 May–25 Jun	None
Total					2330		

the operational sounding sites operated by Taiwan used the Vaisala RS80A (hereinafter RS80) sondes, and the other three used the Japanese-manufactured Meisei RS2-80 (hereinafter MEISEI) sondes. These older sonde types and systems determine the winds using automatic tracking radiotheodolite (ATR) technology. The Vaisala RS92 (hereinafter RS92) and Graw systems determine winds using GPS technology. Four of the enhanced sites used the newer RS92 sondes. The sites using RS80 and RS92 sondes used Digicora version 3.5 ground systems. The other two sites (the southern ship and Laoag) used the German-manufactured Graw DFM-97 sondes. While these four sonde types measure humidity in different ways, all of them except MEISEI are based on the principle that the presence of moisture changes the capacitive characteristics of a sensor. The MEISEI sonde uses a carbon hygristor hygrometer. The operational sites in China used Shang sondes with Goldbeater's-skin humidity sensors, except at the Hong Kong station, which used RS92 sondes. Information on these different sonde types and their humidity biases is presented in Wang and Zhang (2008).

In addition to the 13 sites with upsondes described above, dropsondes from 16 flight missions over the oceans were conducted in the May–June 2008 period. During this period, the research aircraft (Astra SPX jet) released 190 dropsondes over the waters surrounding Taiwan. There is a significant amount of missing data in 30 of the dropsondes, with most of these cases occurring prior to the fourth mission on 29 May. Thereafter, newer sondes were used and the data dropout problem improved dramatically. The primary objective of the dropsonde missions was to document the kinematic and thermodynamic structures of the mei-yu front and the low-level jet offshore the southwest coast of Taiwan in the Taiwan Strait and South China Sea. The Astra jet cruises at ~750 km h^{-1} with flight durations of ~3 h, a ceiling of ~14 km (160 hPa), and about 12–15 drops per mission, with spacing between drops of ~100 km. Additional details of the GPS National Center for Atmospheric Research (NCAR) dropsondes used in these missions can be found in Wang (2005).

A visual inventory of the number of upper-air sondes released on a daily basis during the TiMREX special observing period (SOP; 15 May–25 June) is shown in Fig. 2. In total, 2330 successful sonde observations were made. Of this total, 462 were standard operational and 1868 were supplemental to meet the experiment objectives. Nine intensive observing periods (IOPs), with more frequent sonde launches, were conducted during the SOP. IOPs 3–7 actually make up an enhanced observing period (EOP) from 30 May to 6 June, during which many of the

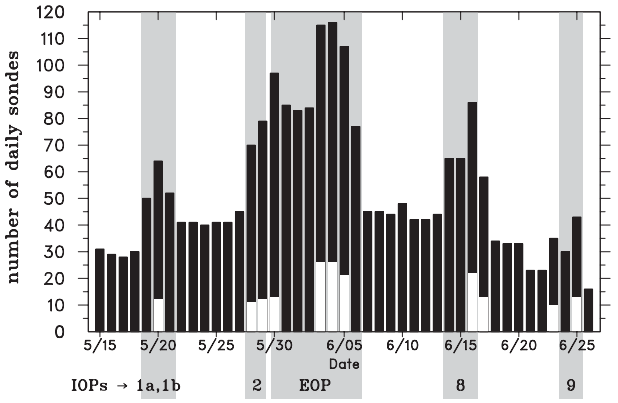

FIG. 2. Time series of daily number of successful sonde launches from the TiMREX sonde network. Black bars show daily total for all sondes, and white bars show total for dropsondes. IOP and EOP days with higher launch frequency are shaded.

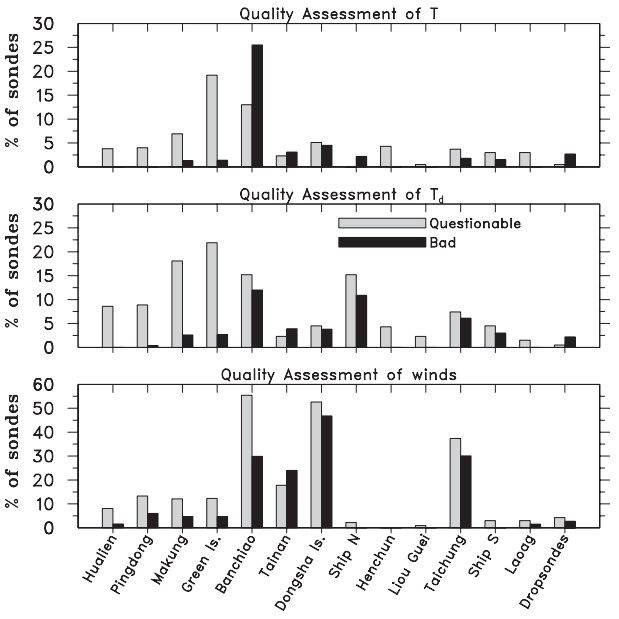

FIG. 3. Assessment of the number of sondes at each site that contain questionable (gray bar) or bad (black bar) data. Humidity errors and near-surface T and T_d errors at ship S (corrected in level 3) are not considered here.

sites launched at a frequency of eight per day (see Table 1 for launch frequency at each site). Over this 8-day EOP, 764 sonde observations were taken from the TiMREX network, which may rival any field experiment for the most sonde observations made over such a limited region. The occasional spikes in the daily sonde count are due to the dropsonde missions.

b. *Stages of QC processing*

The QC procedure used here consists of four stages or levels of data processing. First, the native-resolution (0.5–10 s) sonde data (level 1) were collected from seven different organizations. These data, which were in six different formats, were converted to a common format (NCAR D-file format). Next, these D files were run through the Atmospheric Sounding Processing Environment (ASPEN) software, which performs some limited quality control on the data and produces level-2 (L2) files in NCAR Earth Observing Laboratory (EOL) sounding format. Details of EOL format and the ASPEN QC procedure are described in the L2 sonde documentation available from the TiMREX data archive. In level-3 (L3) processing, problems that are deemed correctable are resolved. Sections 3–6 of this paper describe the identification of the problems in the L2 dataset and their correction to create a L3 product.

The final stage of processing results in a more ''user friendly'' version of the sonde dataset, in which native-resolution L3 data are interpolated onto uniform 5-hPa intervals and QC flags are assigned to each variable to provide a measure of the data's reliability. In this level-4 (L4) dataset, questionable and bad data are identified through application of both objective QC tests as in Loehrer et al. (1996) and the subjective adjustment of QC flags by visual inspection. This latter step represents a type of ''buddy check,'' in which sondes adjacent in time and in close proximity to each other are visually inspected together for continuity of features. By flagging suspect data values, the useful data in these sondes are easily retrievable, with the users deciding what level of quality is acceptable for their analyses. Details of the L4 dataset, including its format and the meaning of the QC flags, are available in a document available from the TiMREX data archive.

After objectively assigning QC flags and their adjustment through visual inspection of individual sondes, an assessment of the number of sondes at each site containing questionable or bad data was done. The results are shown graphically in Fig. 3, where the quality of the thermodynamic (temperature T and dewpoint T_d) and wind variables are considered separately. In general, the sites using MEISEI sondes (Banchiao, Tainan, and Dongsha) have the highest frequency of suspect data. Winds from the sondes at Dongsha Island were particularly problematic, with over 50% of the sondes containing unreliable wind data. In general, sites using GPS wind-finding capabilities (RS92 and Graw systems) had a low frequency of suspect winds, the exception being Taichung which used an older RS92 system and whose sondes may have been impacted by interference from nearby airport transmissions. We note that even at sites at which more than half of the sondes contain suspect data, less than a few percent of the 5-hPa levels are actually affected.

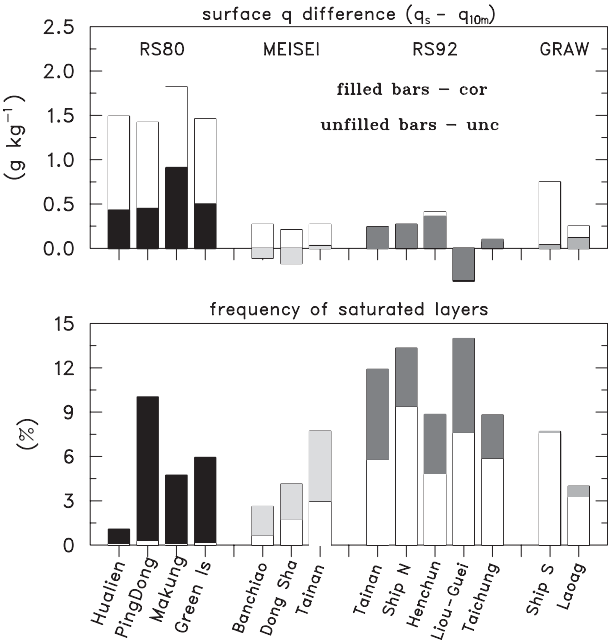

FIG. 4. (top) SOP-mean specific humidity difference between the surface point and the 10-m value from the sonde. (bottom) Frequency of 5-hPa layers that are saturated (RH $\geq$ 100%, with RH computed with respect to ice for $T < 0$°C). White bars are computed with uncorrected data ("unc"), and shaded bars are computed with corrected data ("cor").

3. Sonde humidity biases

An effective means of identifying sonde humidity errors is to compare sonde data with independent observations of the moisture field (from satellite retrievals, surface measurements, etc.). Figure 4 (top panel) shows the SOP-mean specific humidity difference δq between the surface point q_s and that at a point that is located 10 m above the surface (q_{10m}). To facilitate this comparison among the sites, which have a variety of vertical resolutions in their sonde data (see Table 1), the high-vertical-resolution data were used to interpolate q values at 10 m. Note that the surface values are actually from measurements that are independent from the sonde,[1] with the exception of ship *S*, which had no independent surface observations. According to Stull (1988), observed differences of q within the surface layer (10–100 m AGL) under all conditions should not exceed a few tenths of a gram per kilogram. While this is generally the case at sites using MEISEI, RS92, and Graw sondes, the mean δq at the sites using RS80 sondes is considerably larger (>1 g kg^{-1}).

The δq behavior at Liou-Guei needs some additional explanation because the mean negative δq value at this site suggests a physically unrealistic state in which q increases with height above the surface. The cause for this apparent anomalous moisture gradient is that the surface observations at this site were, in fact, not taken at the immediate surface but rather from nearby rooftop measurements. Because the rooftop was ~20 m above the ground level, one would expect the air to be slightly drier there than the sonde observation at 10 m above the ground. This points to the importance of having the surface observation collocated with the sonde release location.

Additional confirmation of a dry bias in the RS80 sondes is seen in the bottom panel of Fig. 4 (unshaded bars), which shows the frequency of 5-hPa layers that are saturated. The frequency of saturated layers at the RS92 sites ranges from about 5% to 10% in the uncorrected data. This is similar to the frequency observed at sites in vicinity of Taiwan during South China Sea Monsoon Experiment (SCSMEX) that was conducted in May and June 1998, and the North American Monsoon Experiment in July and August 2004 (Ciesielski et al. 2009). In contrast, the RS80 sondes exhibit few, if any, saturated layers despite the abundance of convective activity and clouds in this monsoonal environment. The sites with MEISEI sondes also show a lower percentage of saturated layers, which is indicative of a dry bias in these sondes. Further evidence of this bias is seen by noting that Tainan, which used both MEISEI and RS92 sondes (see Table 1), had nearly double the number of saturated layers in RS92 sondes, even though the period with MEISEI sondes was considerably moister in terms of precipitable water (PW; Fig. 6, described below). During TiMREX the frequency and intensity of convection generally decreased from southwest to northeast across the TiMREX domain (not shown), which might partially explain the lower frequency of saturated layers at Banchiao and Hualien.

The analyses presented in Fig. 4 suggest that a significant dry bias is present in the sites using RS80 sondes. To establish the scope and magnitude of the dry bias at these and the other sites, it is useful to compare the PW computed from sonde data with that derived from ground-based GPS measurements or microwave retrievals. Figure 1 (small black circles) shows the location of the GPS sites in Taiwan for which PW could be computed. To facilitate a comparison with sonde data, the 0.5 h–resolution GPS data were averaged into hourly

[1] Surface measurements, independent from sondes, come from nearby surface stations operated by the Taiwanese Central Weather Bureau and Air Force. While instrumentation at these sites is calibrated annually, it is likely that some of the site-to-site variation in the surface q differences in Fig. 4 results from varying distances between the sonde launch point and the location of the surface observation and from different instrument types among the surface sites.

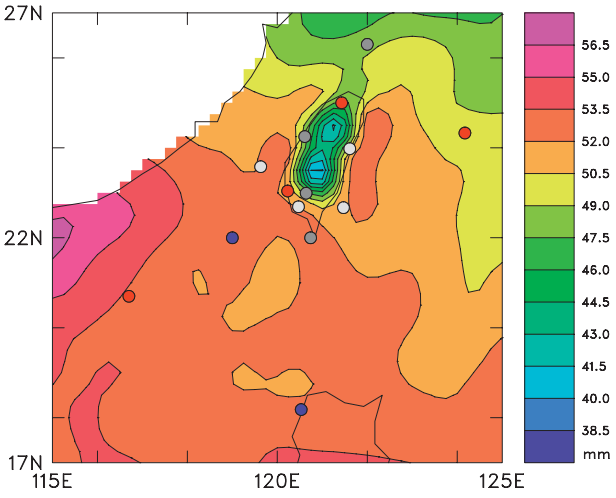

FIG. 5. Merged AMSR-E–GPS analysis of PW (mm) for the SOP of TiMREX. The scale for contours is shown in the label bar on the right. Filled circles indicate locations of sounding sites, with different colors representing different sonde types (refer to Fig. 1).

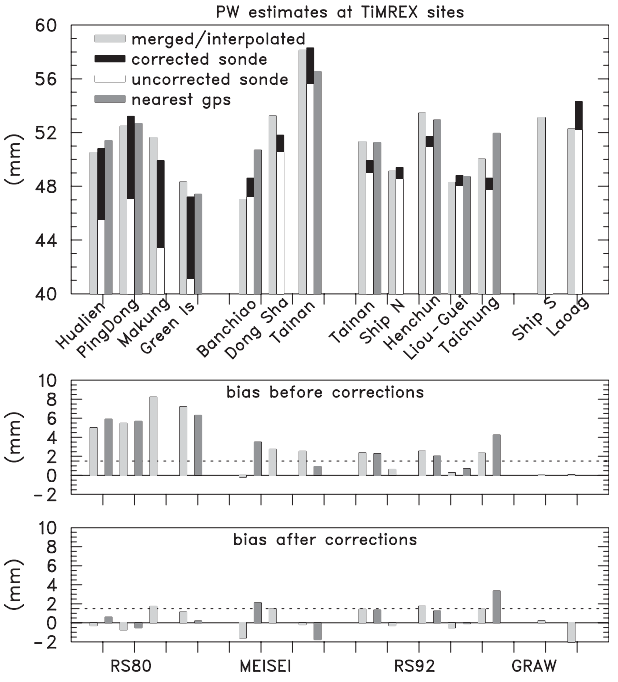

FIG. 6. (top) Comparison of PW (mm) from various estimates [merged analysis in Fig. 5 interpolated to sonde location (light gray bar), uncorrected sonde (white bar), corrected sonde (black bar), and GPS site nearest to sonde site (dark gray bar)] during the TiMREX SOP. Also shown is the PW bias (independent estimate − sonde estimate) (middle) before and (bottom) after corrections, with positive values denoting a sonde dry bias. Horizontal dashed lines in the bottom two panels shows the 95% level above which biases (i.e., the difference in the means) are significant.

bins. For smaller island sites (i.e., Dongsha, Makung, and Green Island) and the research vessels, which had no GPS PW estimates, the Advanced Microwave Scanning Radiometer for Earth Observing System (AMSR-E)-derived PW (available at 0.25° horizontal resolution; online at http://www.remss.com/) can be used at these sites. Because of difficulties with microwave retrievals over land, this product is only available over the oceans. Nominal AMSR-E overpass times are at 0600 and 1800 UTC over the Taiwan region, and estimates are available ~70% of the time. The accuracy of GPS and microwave PW retrievals is ~1–2 mm (Bock et al. 2007; Wentz 1997).

Figure 5 shows an analysis of the SOP-mean PW obtained by merging the AMSR-E data over the ocean and GPS estimates over land using a multiquadric objective interpolation scheme (Nuss and Titley 1994). A minimum in PW is seen over the central mountain range of northern and central Taiwan. If GPS observations of PW were available from locations in the southern mountains, then in all likelihood this minimum would extend farther south to cover this region as well. A maximum in PW occurs off the southern coast of China, with relative maxima over southwestern Taiwan and off its eastern coast. This merged analysis can be used to determine PW for any point in the TiMREX domain.

Figure 6 shows a comparison of mean PW for each of the sounding sites, computed using 1) sonde data, 2) the merged analysis in Fig. 5, and 3) the closest GPS site if one existed within a 50-km radius of the sonde location. The PW means shown here were computed only for periods in which both the GPS and sonde data were present (see Table 1 for days on which sonde data were present at each site). In addition, PW means were adjusted for elevation differences between GPS and sonde sites. If the GPS site was higher than the sonde site, the sonde PW computation began at the height of the GPS site. On the other hand, if the GPS site was lower than the sonde site, the GPS estimate was adjusted by a factor to account for this difference. For example, the elevation of the Liou-Guei sonde site was 266 m, whereas the nearest GPS site was at 187 m. Thus, the nonsonde estimates were multiplied by 0.97 to account for this elevation difference, where this factor was determined as the ratio of PW computed with 266 m as the starting elevation to that computed with 187 m using sonde data from Pingdong.[2]

[2] Pingdong was the nearest sonde site to Liou-Guei, being only 37 km away from Liou-Guei (with both sites situated in the foothills of the Central Mountain Range) and directly upstream (or southwest).

The middle panel of Fig. 6 shows the bias or difference (independent estimate − sonde PW) with a sonde dry bias indicated by a positive value. With standard deviations of these PW estimates ranging from 7 to 9 mm, differences in their means of ~1.5 mm are significant at the 95% level (indicated by the horizontal dashed line). From this analysis the dry bias in the RS80 sondes is readily evident (middle panel), ranging from 5.6 mm (11%) at Pingdong to 8.2 mm (16%) at Makung. The MEISEI sondes appear to have a small dry bias (2%–5%), consistent with the earlier analysis presented in Fig. 4 (bottom panel). The comparison shows little bias at the Graw sites and a slight (a few percent) dry bias in the RS92 sondes, which primarily comes from the daytime sondes, as will be shown later. Analysis of the small number of RS92 sondes launched at Pingdong, Dongsha, and Green Island (see Table 1), share bias characteristics (not shown) that are similar to the ones presented here, namely, small daytime dry biases.

4. Humidity correction schemes

a. Sonde intercomparison studies

During the field phase of TiMREX the dry bias at the RS80 sites was recognized early on, such that a series of intercomparison launches were conducted at Pingdong in June 2008 in which the more reliable RS92 sondes were flown on the same balloon as the RS80 sonde. The RS92 sondes have been shown to have little nighttime moisture bias and a well-documented daytime dry bias (Vömel et al. 2007; Yoneyama et al. 2008; Cady-Pereira et al. 2008, hereinafter CP08). The objective of these launches was to document the atmosphere as broadly as possible (day/night; wet/dry). This exercise ended up yielding 10 daytime and 8 nighttime launches (6 rainy, 3 cloudy, and 9 fair). This dataset of 18 intercomparison launches will be used in conjunction with the cumulative distribution function (CDF) matching method (Nuret et al. 2008; Ciesielski et al. 2009) as the basis for one approach to correcting the dry bias at the RS80 sites.

In addition, 12 intercomparison launches were conducted at Banchiao in 2008 with the MEISEI, Graw, and RS92 sondes flown on the same balloon. These launches were not taken in monsoonal conditions, but rather in April (4) and October (8), and thus they provide a less-than-optimal dataset for developing a correction of MEISEI and Graw sondes. Mean conditions during the intercomparison launches in April and October were drier (5%–20% at any given level) and cooler (0.5°–2°C) than during the SOP, such that the CDF correction table based on this dataset did not span the full parameter space needed to provide a robust correction for the SOP sondes. A preliminary analysis from this limited set of intercomparison launches shows the following: 1) only the RS92 sondes attained saturation in clouds; 2) consistent with the analysis presented in the previous section, the biases in the MEISEI and Graw sondes are considerably smaller than those found in the RS80 sondes; and 3) the MEISEI sondes are insensitive to low RH values such that the Meisei system software typically maintains a near-constant RH above 300 hPa (i.e., the 300-hPa RH value is assigned to all higher levels). The poor response of the MEISEI hygrometer at upper levels is a typical feature of the carbon hygristor (Wang et al. 2003).

b. Use of the intercomparison datasets to develop a humidity correction

The intercomparison datasets described above are used with the CDF matching method to define appropriate correction tables. This method attempts to match the statistics of the problem sondes (e.g., RS80) to those of the reliable sondes (i.e., RS92). The details of this method can be found in Nuret et al. (2008) and Ciesielski et al. (2009). Because previous studies have shown that the RH bias varies with height (or temperature), a differential bias correction is computed in 20°C temperature bins between +40° and −80°C. Application of the CDF matching method corrects the problem sondes to the standard of the RS92.

As seen in Fig. 7, the CDF analysis was refined by creating separate day and night bias correction tables. Further segregation of the training dataset to reflect different environmental conditions (clear, cloudy, and rainy) is limited by the size of the dataset (10 daytime and 8 nighttime samples), and thus was not undertaken. Note, however, that the two maxima in the daytime correction table at temperatures >20°C may reflect a rainy or drier correction scenario. Also seen here for temperatures >0°C is that the bias correction peaks near 10% for RH values of ~70% (night) and at ~8% for RH values of ~65% (day). For temperatures <0°C, the nighttime bias correction gradually increases with colder temperatures, peaking near 25% in the temperature interval from −60° to −80°C for RH values of ~40%. Also shown in Fig. 7 are the 5% and 95% CDF isolines, which provide information on the correction validity range (i.e., 90% of the RS80 intercomparison observations are located between the two lines).

Using the intercomparison dataset taken at Banchiao, day and night correction tables (not shown)[3] were created

[3] The MEISEI and Graw bias correction tables can be found in the L3 sonde dataset documentation available at the TiMREX data archive link listed at the end of this paper.

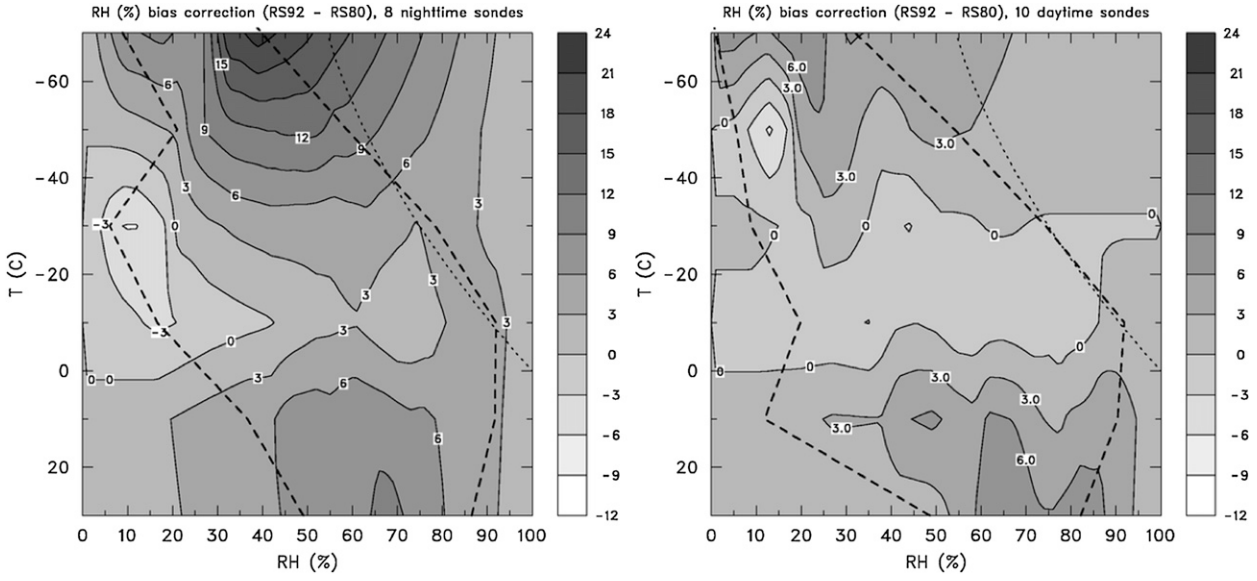

FIG. 7. RH bias corrections (%, contour increment of 3%) for (left) night and (right) day over the full range of temperatures created by matching the RS80 and RS92 CDFs. The axes are temperature and relative humidity as observed by RS80 sondes. Light dotted lines represents saturation with respect to ice. Dashed lines correspond to 5th and 95th percentiles (5% and 95% RS80A CDF isolines, respectively).

for MEISEI and Graw sondes, respectively, to match the statistics of the more reliable RS92 sondes. The nighttime MEISEI sondes have a modest dry bias (~6%) at warmer temperatures and moister conditions. This bias likely accounts for the lack of saturation in these sondes. In dry conditions, the hygrometer on the MEISEI sonde is relatively insensitive to changes in moisture, as can be seen in Fig. 8, which shows a relative lack of low RHs in MEISEI sondes in comparison with the RS92 sondes. This leads to moist bias relative to the RS92 sondes at upper levels. Because of its insensitivity in dry conditions, no CDF corrections to MEISEI sondes were made for low RH values (i.e., RH < 33%). The Graw correction tables (not shown) have a small (3%–6%) dry bias in very moist, warm conditions and a modest moist bias (6%–10%) in drier, cooler conditions. The dry biases in both the MEISEI and Graw sondes are smaller for the daytime sondes, reflecting the daytime dry bias within the RS92 sondes.

c. *Vaisala's testing and development of corrected humidity coefficients for RS80 sondes*

An alternative approach to correcting the RS80 sondes via the CDF matching method came about through a series of laboratory tests conducted by Vaisala. Recognizing the significant dry bias of the RS80 sondes during TiMREX, a sample of 70 RS80 sondes selected from different production batches was returned from Taiwan to Vaisala for further investigation. Upon testing, Vaisala determined that the dry bias in the sondes at three sites (Pingdong, Makung, and Green Island) was indeed beyond what was typical and that its cause was an unusually high level of contaminants on the humidity sensors, which reduces their ability to absorb water vapor. Such contamination problems were the main source of a dry bias in RS80H sondes in the Tropical Ocean and Global Atmosphere Coupled Ocean–Atmosphere Response Experiment (TOGA COARE; Wang et al. 2002), which was found to increase with the sonde's age. In the African Monsoon Multidisciplinary Analyses (AMMA) field experiment, many of the RS80 sondes were up to 9 yr old, resulting in dry biases of ~15% in the lower troposphere

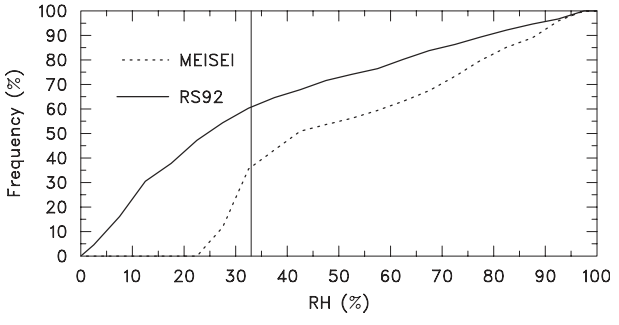

FIG. 8. RH CDFs computed over all temperatures for RS92 sondes (solid line) and MEISEI sondes (dotted line) from 12 intercomparison launches conducted at Banchiao. Note the rapid decrease in MEISEI CDF for RHs < 33% resulting from the insensitivity of the Meisei humidity sensor at low RH.

(Nuret et al. 2008). The majority of the RS80 sondes used in TiMREX were less than 1 yr old, such that the magnitude of their dry bias is somewhat surprising. For example, the RS80 sondes at Pingdong, Makung, and Green Island were manufactured in the autumn of 2007, and ~70% of the sondes launched at Hualien were manufactured in the autumn of 2006, with the remainder from 2007 and 2008 productions.

The sondes collected by Vaisala were given a heat treatment to burn off the contaminants and then were recalibrated. This resulted in a set of corrected calibration coefficients. Using a statistical average correction for these 70 sondes, Vaisala was able to provide corrected humidity coefficients for the RS80 sondes used during TiMREX at the three sites mentioned above. For whatever reason, Vaisala did not feel that the sondes used at Hualien were affected and no corrected coefficients were provided for this site. As discussed in detail in section 5a, the sondes at Hualien are corrected using the CDF matching method described above, whereas the sondes from the other three RS80 sites make use of the corrected coefficients provided by Vaisala.

d. Daytime dry bias correction

Many studies have shown a notable daytime dry bias in Vaisala sondes attributed to solar heating of the sonde humidity sensor. Such a correction is necessary at nearly all of the upsonde sites in TiMREX because the sonde type either was Vaisala or was corrected to the standard of the RS92 sonde via CDF matching. No daytime dry bias has been observed in dropsondes—likely because of their high descent rate, which provides excellent ventilation. In this section, we consider two methods for correcting the daytime dry bias.

Using comparisons between PW retrieved from a microwave radiometer and that from sonde data at the Atmospheric Radiation Measurement Program (ARM) Southern Great Plains site, CP08 was able to isolate the daytime heating effect and develop a correction for different Vaisala sonde types. Despite a protective covering on the RS80-H humidity sensor to shield it from precipitation and radiative effects, a daytime dry bias is observed. As reported in CP08, later-model Vaisala sondes (RS90 and RS92), which lack this covering, have a more pronounced daytime bias than the RS80 model. The daytime RS80 moist bias in the range from −20° to −40°C (i.e., negative bias values in the right panel of Fig. 7) likely reflects this larger daytime dry bias in the RS92 sondes, consistent with the findings of CP08. In their study, no attempt was made to determine a height-dependent correction.

Their daytime heating correction has the following form:

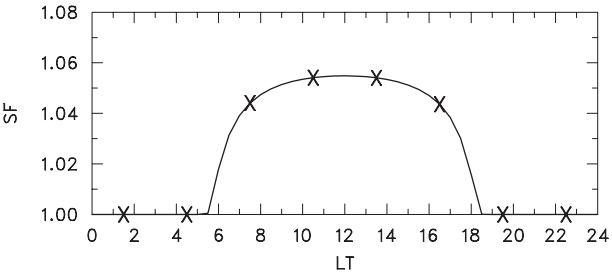

FIG. 9. The scale factor (SF) for correction of sonde water vapor mixing ratio r as a function of local time (LT) for RS80 sondes released at the position of Pingdong on 1 Jun; The "x"s indicate the SF applied to the sondes launched at 8 times per day.

$$\mathrm{SF} = 1.0 + \alpha \exp(-0.2/\cos\theta), \tag{1}$$

where SF is a scale factor that multiplies water vapor mixing ratio r at each level, α is a constant (0.067 for RS80 and 0.093 for RS92), and θ is the solar zenith angle, which is function of the station's latitude, longitude, time of day, and time of year. For example, Fig. 9 shows the correction that would be applied to the RS80 humidity data at Pingdong on 1 June as a function of time of day. As seen here, only sondes launched between 0530 and 1830 LT are affected, with r values from sondes launched between 1130 and 1330 LT being increased by about 6%. In practice, the daytime correction was applied by converting the dewpoint temperature T_d to an r value, scaling the r value, and then converting the scaled r value back to a new T_d.

By comparing the relative humidity profiles obtained from several contemporaneous launches of RS92 sondes and the Snow White (SW) chilled-mirror hygrometer taken during the *Mirai* Indian Ocean Cruise for the Study of the MJO Convective Onset (MISMO), Yoneyama et al. (2008) determined the vertical profile of the daytime RS92 dry bias as shown in Fig. 10. This profile formed the vertical structure $\mathrm{RH_{dif}}$ for Yoneyama's correction (hereinafter YON), which is given as

$$\mathrm{RH_{cor}} = \{100/[100 + (\cos\theta/\cos\theta_m)\mathrm{RH_{dif}}]\}\mathrm{RH_{obs}}, \tag{2}$$

where θ_m is the mean solar angle (24.1°) of the 14 intercomparison sondes, $\mathrm{RH_{obs}}$ is the observed RH profile, and $\mathrm{RH_{cor}}$ is the corrected RH. Also seen in Fig. 10 is the vertical structure of the correction proposed by Vömel et al. (2007). As can be noted, Yoneyama's correction increases with height but is near zero at low levels, in contrast to Vomel's correction, which is ~9% near the surface. While improvements to the coating of the RS92 humidity sensor may account for the smaller bias in YON's correction, ultimately the reasons for this difference are unclear. In testing the various daytime

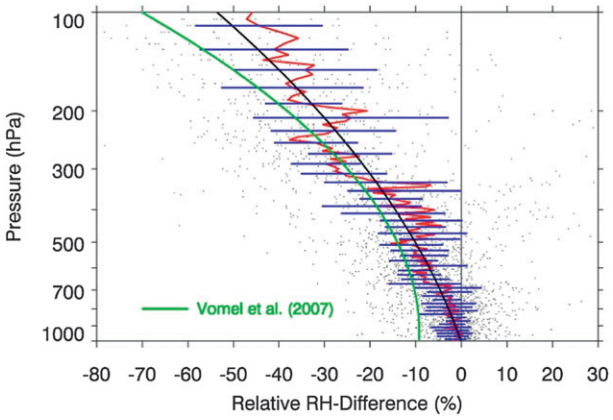

FIG. 10. Relative difference between RH from RS92 sondes and the SW hygrometer for 14 sets of near–local noon observations from MISMO (from Yoneyama et al. 2008). The red line indicates the mean difference profile, blue horizontal lines are the standard deviation, the black curve is a polynomial fit to the mean profile, and the green line is the correction profile proposed by Vömel et al. (2007).

corrections on the RS92 sondes, it was found that YON provided the best validation to independent observations (e.g., GPS PW analysis in Fig. 6 and surface q difference in Fig. 4a), with the other corrections producing too much moistening in the lower troposphere.

e. Sequence of corrections

At many of the sites, the correction method is performed as a two-step procedure: application of the CFD method to correct the sonde to the standard of the RS92 followed by a daytime correction. A variation to this procedure was tested but ultimately not used. In this variant approach, the order of the corrections was switched such that the daytime correction was applied to the RS92 sondes from the intercomparison dataset prior to the CDF matching. This produced a daytime reference correction table that when applied resulted in nearly identical correction statistics (i.e., mean PW biases and δq) with the exception that fewer (1%–2%) saturated layers were produced.

5. Application and evaluation of humidity corrections

a. Correction of RS80 sondes

First, we consider the humidity corrections that are applied to the RS80 soundings, which had the largest humidity biases during TiMREX (Figs. 4 and 6). At three of the RS80 sites (Makung, Green Island, and Pingdong) we have two options for correcting the dry bias: 1) application of the CDF matching method using the Pingdong intercomparison dataset, or 2) use of the Vaisala corrected coefficients (VCC). Because corrected coefficients were not produced at Hualien, we have no choice at this site but to use the former method. By applying both methods to the three RS80 sites in question, it was found that using the VCC resulted in more realistic moisture statistics with a greater frequency of higher RHs than the CDF matching method. For example, with the VCC the frequency of saturated layers was ~5% greater and the mean PW was ~1 mm higher. At Pingdong, the VCC resulted in slightly better agreement with independent estimates, with an RMS PW difference (GPS − corrected sonde) of 0.74 mm for CDF-corrected sondes and 0.56 mm using the VCC. For this reason, the VCC were used to correct the humidity data at the three sites for which the corrected coefficients were available. After application of the VCC, the CP08 correction was applied to address the daytime dry bias in the RS80 sondes. At Hualien, the CDF method was used, which corrects the sondes to the standard of the RS92, followed by application of the CP08 correction for RS92 sondes. In applying the daytime corrections (using CP08 for the RS80 sondes and YON for the others), the following restrictions are imposed: T_d should not exceed T such that RH was limited to be ≤100% for $T > 0$°C and up to 130% for $T < 0$°C.

Application of the correction schemes described above to RS80 sondes substantially moistens the soundings, resulting in more-realistic near-surface gradients of q (shaded bars in top panel of Fig. 4). The correction resulted in a reduction in the SOP-mean δq for the RS80 sites from values of 1.4–1.8 g kg^{-1} to a more reasonable range from 0.4 to 0.9 g kg^{-1}. The frequency of saturated layers (bottom panel Fig. 4) increased from near zero in the uncorrected data to 5%–10% with corrections. The exception to this is at Hualien, which shows only a slight increase in saturated layers, suggesting that the corrected humidities—in particular, at upper levels—are likely too low at this site.

The impact of the correction on SOP-mean PW is shown in Fig. 6 (bottom panel). In the uncorrected sondes, the dry bias ranges from 5 to 8 mm in terms of PW (positive values in middle panel). With the corrected humidities, the biases are less than 2 mm or within the accuracy of the independent estimates. While Makung sondes have been substantially improved by the corrections, they still appear to have a slight dry bias with a corrected PW bias of 1.7 mm and δq of 0.91. Overall, these favorable comparisons for the corrected RS80 sondes to independent humidity estimates give us confidence that the corrections have significantly improved the description of the moisture field.

Because of the importance of the Pingdong soundings in cross validating other observations in the core of the

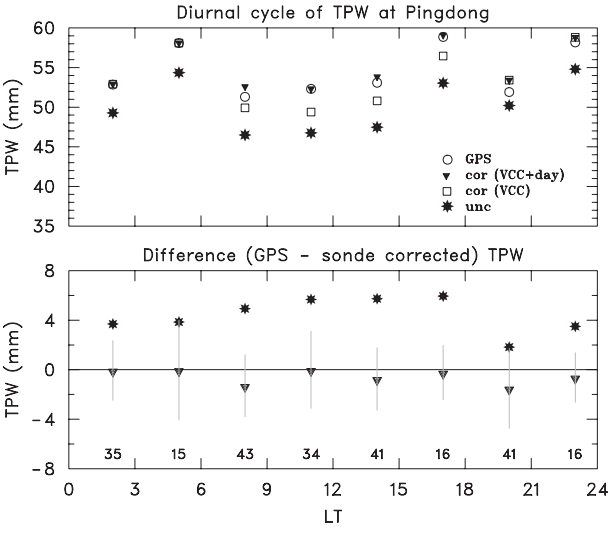

FIG. 11. (top) Diurnal cycle of PW from a GPS site near Pingdong (open circles) and from uncorrected (asterisks) and corrected (squares: VCC only; triangles: VCC and daytime correction) Pingdong sonde data. The x axis is local time (LT). (bottom) Diurnal cycle of PW difference (GPS − corrected sonde) for uncorrected (asterisks) and corrected (triangles) sonde data. Triangle symbols show the mean of corrected data, vertical lines show standard deviation, and the number near the bottom of the frame indicates the number of comparison observations contributing to the average at a given LT.

enhanced observational domain of TiMREX [specifically its close proximity to the S-band dual-polarization Doppler radar (S-POL) and the TiMREX supersite in southern Taiwan], the validation of its humidity corrections is given special attention here. Application of the VCC and daytime heating correction to the Pingdong RS80 sondes during TiMREX increased the SOP-mean sonde PW from 48.2 to 54.4 mm (~12%). The nearest GPS site with a near-complete data record during the SOP was 17 km to the southwest of the Pingdong station and toward the coast. Matching only contemporaneous observations from the sonde to 3-h mean values from the GPS site yields means of 53.2 and 52.3 mm, respectively, or a difference of 0.9 mm. Taking into account the sonde's lower starting elevation (19 m, vs 46 m for the GPS site) further reduces the difference to 0.5 mm. The temporal correlation coefficient between the 3-h GPS and sonde-corrected PW values is 0.95, with a regression-line slope of 0.97 and an intercept of 1.6 mm. This excellent agreement between sonde-corrected PW and the independent GPS-based values, in both a mean and temporally varying sense, indicates that the correction scheme has effectively removed the dry bias in the Pingdong soundings.

Further details of the correction are seen in Fig. 11, which shows the diurnal cycle of PW at this GPS site and that computed with uncorrected and corrected Pingdong sonde data. This analysis considers only times at which both GPS and sonde estimates were available. As one can see, the diurnal cycle of PW in the corrected sonde data closely matches that of the GPS estimate, with differences at individual times (bottom panel) of less than 2 mm. With uncorrected sonde data the differences are generally between 4 and 8 mm at individual hours. This analysis also shows the impact of the daytime dry bias, with larger differences during the daytime hours, and the importance of applying a daytime heating correction to mitigate this problem.

The higher-than-average values of PW at 0500, 1700, and 2300 LT (top panel of Fig. 11) result from the particular sampling that went into these hours. For example, sonde launches at these times were conducted only on IOP days with eight sondes per day (note the smaller sample size at these hours as indicated by the numbers in bottom panel of Fig. 11), and these enhanced observing periods tended to be wetter and more convectively active than non-IOP days (not shown). On non-IOP days, Pingdong had regular sonde launches at 0200, 0800, 1100, 1400, and 2000 LT during the SOP.

b. *Corrections for other sonde types*

In comparison with the RS80 sondes, the humidity biases in the other sonde types are considerably smaller. Because the biases are relatively small for the MEISEI and Graw sondes and their correction schemes are less than optimal, as described above, the necessity of correcting these sondes may be questioned. In the end, the corrections were performed and both the corrected and uncorrected datasets are made available, giving users the option of which dataset they prefer to use.

Separating the PW comparisons in Fig. 6 by time of day for the RS92 uncorrected sondes shows that the PW bias (GPS − sonde) for the daytime sondes is 2.9 mm as compared with 0.7 mm for the nighttime sondes. The daytime nature of this bias is evident in Fig. 12, which shows a diurnal comparison of PW using the Taichung sondes with a nearby (8.5 km) GPS site. Little nighttime bias is seen whereas daytime PW differences range from ~2 to 5 mm in the uncorrected sonde data. Application of the YON correction reduces the dry bias by ~50% but does not entirely remove it. As seen in Fig. 6, three of the RS92 sites (Tainan, Henchun, and Taichung) still have a small dry bias in the corrected data, primarily resulting from undercorrected daytime sondes. Applying the CP08 correction overmoistens the low levels, producing unrealistic negative δq at the surface (i.e., a q increase with height; see Fig. 4). For this reason, the YON correction was used in the RS92 sondes, which

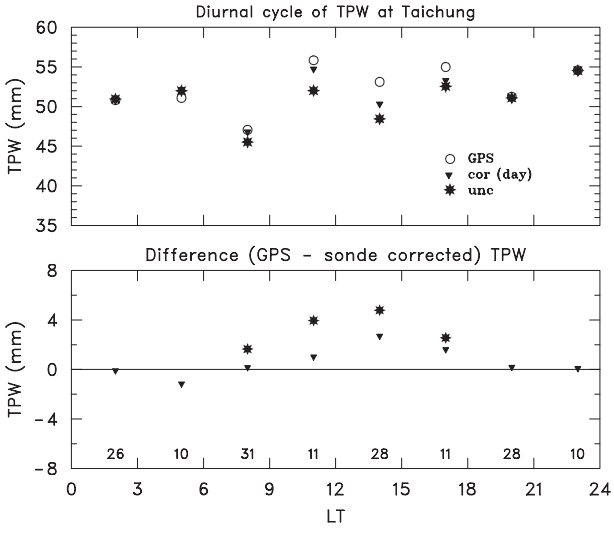

FIG. 12. As in Fig. 11, but from a GPS site near Taichung. At this site the only correction applied was for daytime heating (triangles in both panels).

produces more realistic moisture profiles and a slight increase (~1 mm) in the mean PW (Fig. 6).

For the MEISEI sondes the correction scheme involved application of the CDF method using the intercomparison dataset of RS92 and MEISEI sondes taken at Banchiao, followed by the YON daytime correction. Recall that the CDF method is not applied for RH < 33% (see Fig. 8) for doing so would introduce a significant dry bias in the MEISEI sondes above 300 hPa. Examination of Figs. 4 and 6 suggests that the corrections were generally beneficial in increasing the frequency of saturation and reducing the slight dry bias observed in PW in the MEISEI sondes. On the other hand, the negative or near-zero δq in the corrected MEISEI sondes (top panel of Fig. 4) suggests that the correction likely overmoistened the low levels.

Laoag appears to have a slight dry bias, as seen in lower-than-expected frequency of saturated layers. Thus, at this site we apply the CDF method using the intercomparison dataset of RS92 and Graw sondes taken at Banchiao. Having corrected the Graw sondes to the standard of the RS92, the daytime YON correction is then applied. The corrections at this site produce a slight reduction in δq, a small increase in the frequency of saturated layers, and a 2-mm increase in the mean PW. While the PW comparison for this site in Fig. 6 would suggest that the correction introduced a slight moist bias in the Laoag sondes, the uncertainty of the independent PW product is larger for this location because it is based on an oceanic satellite product (i.e., ASMR-E) that is interpolated over land. The corrections of the thermodynamic data from ship *S* (99810), which used Graw sondes, are considered in the next section.

The last column in Table 1 summarizes the corrections that were applied to the various sonde types at each site. The corrections used were those that resulted in the best comparisons to independent data sources. While the need for corrections in the MEISEI and Graw sondes is marginal and their correction scheme is less than optimal, corrected datasets for these sondes were created to be used at the researcher's discretion.

6. Correction of low-level T and T_d at south ship *S* (99810)

Inspection of the data at ship *S* (99810), using the standard metrics to identify humidity errors (frequency of saturated layers, surface δq, comparison of sonde PW with independent estimates), suggests that little to no humidity bias is present at this site. However, visual inspection of these sondes revealed that a significant fraction of them (80%–90%) have thermodynamic data in the lowest levels (from the surface up to 100–300 m) that were of questionable quality. An example is shown in Fig. 13, which shows unrealistically large gradients of T and T_d in the lowest 300 m, with a T change of 11.6°C in this layer. The cause of these questionable data is unclear but likely is related to contamination from the ship structure—perhaps the heating of the ship structure, because the problem was most pronounced in daytime sondes—or the release of the sonde package in the exhaust plume from the ship stack.

Because the contaminated data can readily be identified by large, unrealistic gradients in T and T_d in the lowest levels, a procedure was developed to correct these questionable data values. In this procedure, a visual sonde editor[4] is used to mark the questionable data in the 5-hPa interpolated sonde (L4.0) dataset. The vertical gradient of T and T_d is then computed with a one-sided, second-order derivative using the good-quality data immediately above the questionable data. For example, the temperature gradient is computed as

$$dT/dz_k = -T_{k+2} + 4T_{k+1} - 3T_k/(z_{k+2} - z_k), \quad (3)$$

where k is the index of the first T value in the 5-hPa file considered to be of good quality. This gradient is then used to extrapolate corrected T values down to the surface in following fashion:

[4] The interactive software tool xsnd (examine sonde) was designed to allow visual inspection of a sounding and adjustment of the quality flags of each data point by merely clicking on it.

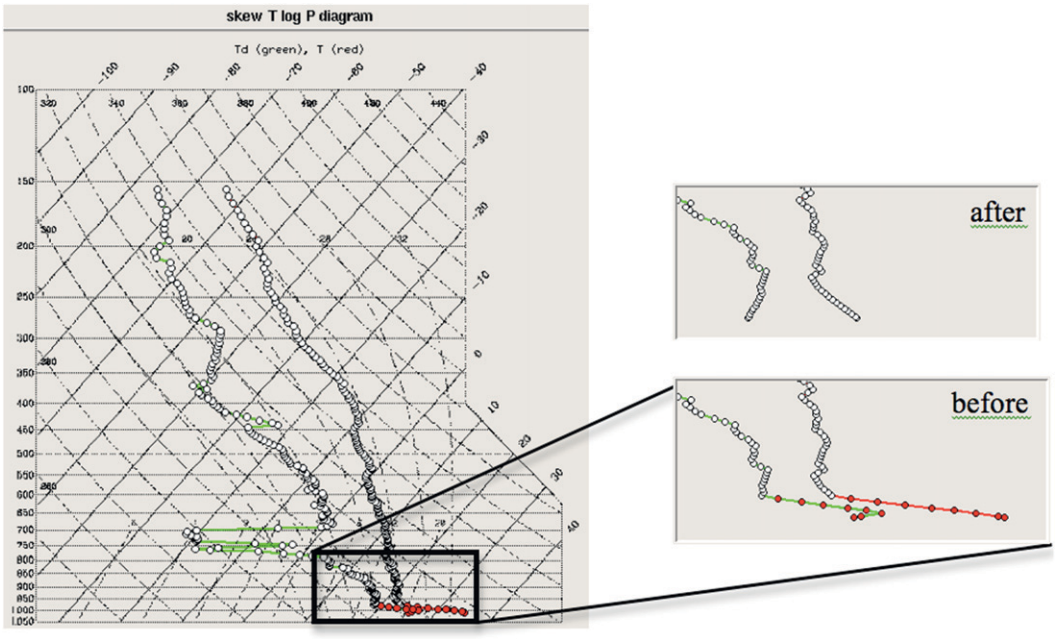

FIG. 13. Example of temperature and moisture data from the research vessel ship *S* (99810) sounding taken at 0600 UTC 16 May 2008 that was contaminated by the ship structure. Contaminated points, identified by large and unrealistic gradients near the surface, are indicated by red filled circles. The inset shows the lower levels of the sounding before and after the correction described in the text.

$$T(z) = T_k + dT/dz_k(z - z_k). \quad (4)$$

Using this simple procedure we corrected the T and T_d in all of the ship sondes that had low-level values that were marked as being questionable. These corrections are present in both the L3 (native vertical resolution) and L4 (5-hPa interpolated) datasets for this site. The inset in Fig. 13 shows how the low-level data have been corrected in the 0600 UTC 16 May sounding. As one can see, the large gradients in these fields have been replaced by a realistic-looking mixed layer structure. In this example the surface air temperature T_s was decreased by ~7°C by the correction. In general, the magnitudes of the corrections are more modest in size, with a mean T_s correction of ~2°C, as shown in Table 2. This table summarizes the impact of the correction by listing the mean depth over which the correction was applied and the RMS correction at the surface (i.e., the uncorrected value minus the corrected value). Of the 134 sondes taken at 99810, 80.6% had questionable T data near the surface and 92.5% had questionable T_d. The correction resulted in a decrease in T_s in all but four cases, and in all cases the correction led to a decrease in surface T_d. The diurnal variation of the correction in terms of magnitude and depth applied is also listed in Table 2. Note that the corrections were largest in magnitude and extended over the greatest vertical depth in the afternoon (0600 UTC) sondes, lending credence to the notion that heating of the ship structure contributed to the poor quality of the data near the surface.

To estimate the magnitude of errors produced by the correction procedure, we have applied it to sondes for which no contamination problems were observed. Here the correction was applied over the lowest 20 hPa of the sounding, and Table 3 examines the RMS corrections

TABLE 2. Characteristics of the low-level T and T_d corrections at ship *S* (99810) as function of sounding time, showing number of sondes corrected, RMS correction at surface (i.e., uncorrected value − corrected value), and mean depth over which correction was applied.

	T			T_d		
Time UTC (LT)	No.	RMS correction (°C)	Depth (hPa)	No.	RMS correction (°C)	Depth (hPa)
All times	108	2.02	17.0	124	2.18	17.8
0000 (0800)	31	1.74	16.0	34	2.31	17.2
0600 (1400)	32	2.90	24.0	33	2.71	23.6
1400 (2000)	23	1.64	14.8	28	1.79	15.0
2000 (0200)	21	1.61	14.5	28	1.85	14.6

TABLE 3. Estimate of errors produced by correction (see text for details).

	T		T_d	
Site	RMS correction (°C)	No. sondes	RMS correction (°C)	No. sondes
Ship *S* (99810)	0.09	26	0.21	10
Dropsondes	0.03	173	0.02	155

at the surface. Because the sample size of the sondes without quality issues at 99810 is small, we also examined the correction procedure on the dropsondes. Here, only dropsondes with good T and T_d data down to the surface were used. From these results it appears that the correction procedure preserves the low-level gradients well, with errors in surface T and T_d on the order of 0.2°C or less.

To check the reasonableness of the correction, Fig. 14 shows the impact of the correction on the SST − T_s difference. Here the SST data have been estimated from AMSR-E satellite retrievals because the ship did not record this data variable. Under typical conditions over the tropical oceans with a turbulent mixed boundary layer, one would expect the temperature and moisture values at the surface to decrease slightly with height. However, without the correction the SST − T_s difference is generally negative (i.e., $T_s >$ SST), with a period mean of −0.63°C. With the correction, the mean difference shows a more reasonable value of 0.94°C. This corresponds well to the mean difference of 0.85°C observed from the two research vessels in SCSMEX, which took sounding observations during May and June 1998 over the South China Sea. In addition, Fairall et al. (1996) showed a mean SST − T_{10m} difference of about 1.5°C over the west Pacific warm pool region during the TOGA COARE period. Times with larger positive differences in the corrected data in Fig. 14 generally correspond to periods of rainfall during which rain-cooled air is present near the surface. Even in the corrected data, there are still 11 soundings with small negative differences. During SCSMEX, there were periods over the northern South China Sea after the monsoon onset that were characterized by small negative differences (see Fig. 5 of Ciesielski and Johnson 2009). Such conditions existed at times during SCSMEX when warm, moist air advected over cooler waters resulting in very small or negative buoyancy fluxes and thus weak upward mixing of heat and moisture from the ocean surface. In other words, in the postmonsoon environment in this region there is a precedent for conditions of small negative SST − T_s differences to exist, but not of the magnitude observed in the uncorrected data.

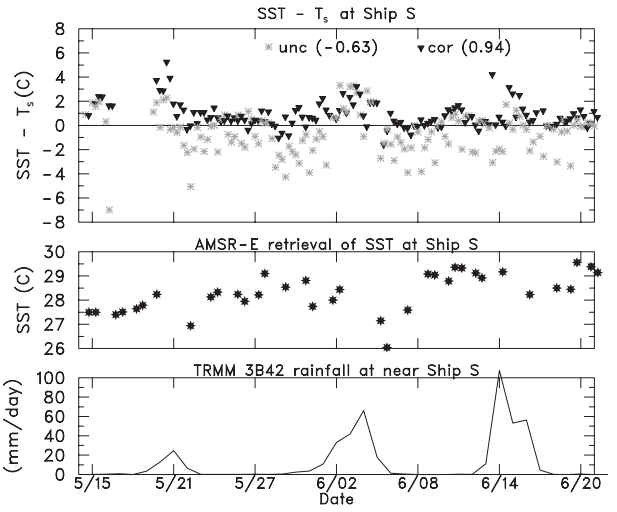

FIG. 14. Time series during TiMREX. (top) SST − surface temperature T_s at 99810 for corrected (black symbols) and uncorrected (gray asterisks) T_s. The numbers in parentheses represent the mean SST − T_s difference for the period. (middle) AMSR-E retrieval of SST interpolated to ship position. (bottom) Rainfall in the vicinity (1° radius) of the ship.

7. Impacts of the corrections

This section considers the impact of the corrections described above on various moisture analyses, as well as its effect on the properties of convection. All RH analyses presented in this section show RH computed with respect to ice for temperatures below freezing.[5]

Figure 15 shows the magnitude of the corrections on the SOP-mean RH and q profiles for the four sonde types in this study. As one might expect, the corrections in the RS80 sondes are the largest of all of the sonde types, with RH corrections of ~10% (or 2 g kg^{-1}) near the surface, decreasing to ~5% at upper levels. In the RS92 sondes, the RH correction is very small at low levels and increases to ~20% at upper levels. In terms of q, the correction maximizes at midlevels at ~0.25 g kg^{-1}. The corrected RS80 and RS92 sondes have similar mean profiles in the low levels with near-surface values of approximately 80% and 17 g kg^{-1}. Above 400 hPa the corrected RS92 sondes have higher RH by some 30% than the RS80 sondes, although in terms of absolute moisture q these upper-level differences are small. Part of the reason for this RH difference is that the CP08 correction used on the RS80 sondes is essentially constant in height whereas the YON correction used on the

[5] Here, RH = e/e_s, where e is vapor pressure and e_s is the saturation vapor pressure. For $T \geq 0$°C, e_s is computed as e_s over water; for $T < 0$°C, e_s is computed as e_s over ice.

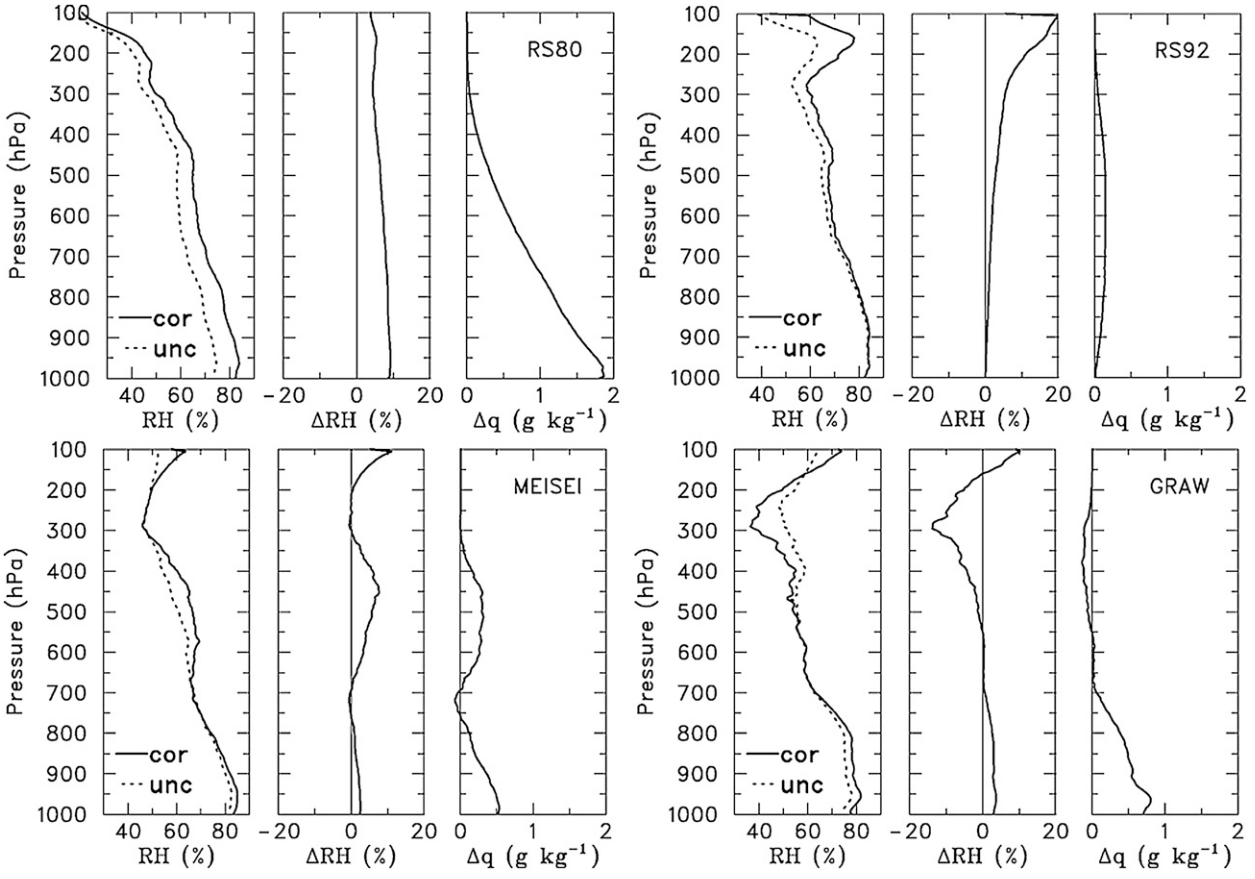

FIG. 15. Magnitude of humidity corrections for various sensor types: (top left) RS80, (top right) RS92, (bottom left) MEISEI, and (bottom right) Graw at Laoag. For each group of three panels, the curves show the mean SOP profiles of (left) RH and their difference (corrected − uncorrected) for (center) relative humidity with respect to ice and (right) specific humidity.

RS92 sondes increases with height, being largest at upper levels (Fig. 10). In this monsoonal environment, the moist upper-level conditions of the RS92 sondes are likely a better depiction of reality. The RS80 sondes at these levels are likely undercorrected, which is consistent with their lower percentage of saturated layers shown in Fig. 4. The corrections at the MEISEI sites and Laoag (the only Graw site considered here) increase the low-level RH by a few percent (or ~0.5 g kg^{-1}). Above 700 hPa the corrections act to moisten the MEISEI sondes slightly and produce some drying at upper levels in the Laoag Graw sondes. Because the correction schemes for these latter two sonde types are less than optimal, it is not entirely clear whether all of the changes produced by the corrections are actually beneficial (e.g., upper-level drying at Laoag).

As noted in Fig. 15, the humidity corrections in terms of absolute moisture q are a maximum at lower levels. Because of the strong sensitivity of convection to low-level thermodynamic fields (e.g., Crook 1996), Fig. 16 considers the correction's impact on CAPE and convective inhibition (CIN). These quantities were computed assuming pseudoadiabatic ascent using mean thermodynamic conditions in the lowest 50 hPa. In the RS80 sondes the correction results in huge changes in CAPE and CIN: CAPE increases by 484 J kg^{-1} (a threefold increase) and |CIN| decreases by 80 J kg^{-1}. The magnitudes of these changes are very similar to those observed in the Vaisala H sondes in TOGA COARE resulting from the correction made in those sondes (Ciesielski et al. 2003). The changes in the convective parameters in the other sonde types are considerably smaller and are consistent with the smaller corrections depicted in several of the earlier figures. This is also true for ship *S*, except here the low-level T and T_d corrections produce a slight decrease in CAPE and an increase in CIN, which is an opposite trend from the other sites. Table 4 summarizes the mean changes resulting from the corrections in these and some additional convective parameters for each sonde type. For example, for the RS80 sondes the mean PW increases by 5.6 mm (12%), the lifting condensation level (LCL) lowers by 27 hPa, and the level of neutral

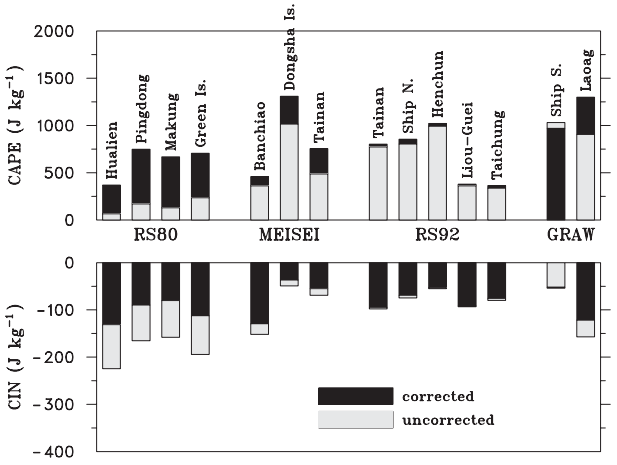

FIG. 16. (top) Mean values of CAPE at sounding sites computed with humidity-corrected (top of black bar) and humidity-uncorrected (top of gray bar) data. (bottom) Mean values of CIN computed with humidity-corrected (bottom of black bar) and humidity-uncorrected (bottom of gray bar) data. Sites are grouped according to sensor type: RS80, MEISEI, RS92, and Graw.

buoyancy (LNB) decreases by 50 hPa. Again, the humidity corrections in the other sonde types produce only modest changes in these parameters. It is worth noting that the variation in mean values of these parameters over the different sonde types is considerably smaller in the corrected data. This improved consistency is also seen spatially between adjacent sites such as Pingdong and Tainan (see the corrected CAPE and CIN in Fig. 16 for these sites) and temporally (see the corrected values at Tainan for the different sonde types). Such consistency gives us confidence that the corrections have, in fact, improved the description of the moisture field.

To explore further the impact of the humidity corrections on convection, we utilize the buoyancy-sorting cloud model of Raymond and Blyth (1992) with the L4 5-hPa dataset. Their model is based on the premise that entrainment and mixing in clouds occur as a random, highly episodic process. In this model, a parcel with mean properties of the 1000–950-hPa layer ascends through the troposphere up to the LNB. At each 5-hPa level the parcel mixes with environmental air with different mixing fractions ranging from 0.1 to 0.9. These diluted parcels then ascend or descend to their nearest level of neutral buoyancy with no overshooting allowed. For the results shown here, we assume that as the parcel ascends and water condenses it can possess a maximum of 3 g kg^{-1} of liquid water. Above this threshold, which represents a midrange value used in Global Atmospheric Research Program (GARP) Atlantic Tropical Experiment (GATE) simulations (Ferrier and Houze 1989), water falls out as precipitation.

The model was applied to individual sondes (both humidity corrected and uncorrected) for the four different sonde types. Model results from the individual sondes, which were required to have good thermodynamic data through the depth of the troposphere, were then averaged into mean profiles for each sonde type. Results from the model for the RS80 sondes are shown in Fig. 17 in terms of vertical profiles of detrainment probability and convective mass flux. The results in the top panels are for the case in which no ice effects are included, whereas the bottom panels show the analyses in which ice formation was allowed, which enhances parcel buoyancy. For these latter results, the model assumes equilibrium ice processes (i.e., all water substance below 0°C is ice).

The large humidity increases in the RS80 sondes depicted in earlier figures (Figs. 4, 6, and 15), have a significant impact on detrainment and convective mass flux. The humidity-corrected RS80 profiles have less detrainment below 600 hPa compensated by a large increase (more than double) above 250 hPa. In the no-ice case there is a secondary peak in outflow layers observed near 400 hPa that is presumably related to a layer of enhanced stability near the 0°C level (Johnson et al. 1996; Zuidema 1998). When ice effects are included (bottom panels), this secondary detrainment peak is no longer present because the additional latent heating resulting from freezing and deposition enhances buoyancy,

TABLE 4. Impact of corrected humidity data on convective parameters computed for the various sonde types in TiMREX. Here, unc = uncorrected, cor = corrected, and Δ refers to the change in a parameter as a result of using the corrected humidity data. The number of sondes is shown in parentheses after each type.

	RS80 (876)			MEISEI (411)			RS92 (445)			Graw (185)		
Parameter	Unc	Cor	Δ	Unc	Cor	Δ	Unc	Cor	Δ	Unc	Cor	Δ
CAPE (J kg^{-1})	153	637	+484	626	829	+203	647	672	+25	646	634	−12
CIN (J kg^{-1})	−180	−101	+80	−92	−76	+16	−80	−77	+3	−67	−66	−1
PW (mm)	46.6	52.2	+5.6	51.9	53.6	+1.7	51.9	52.6	+0.7	52.3	52.8	+0.5
LCL (hPa)	900	927	+27	929	938	+9	921	923	+2	924	926	+2
LNB (hPa)	229	179	−50	186	173	−13	177	178	+1	181	185	+4

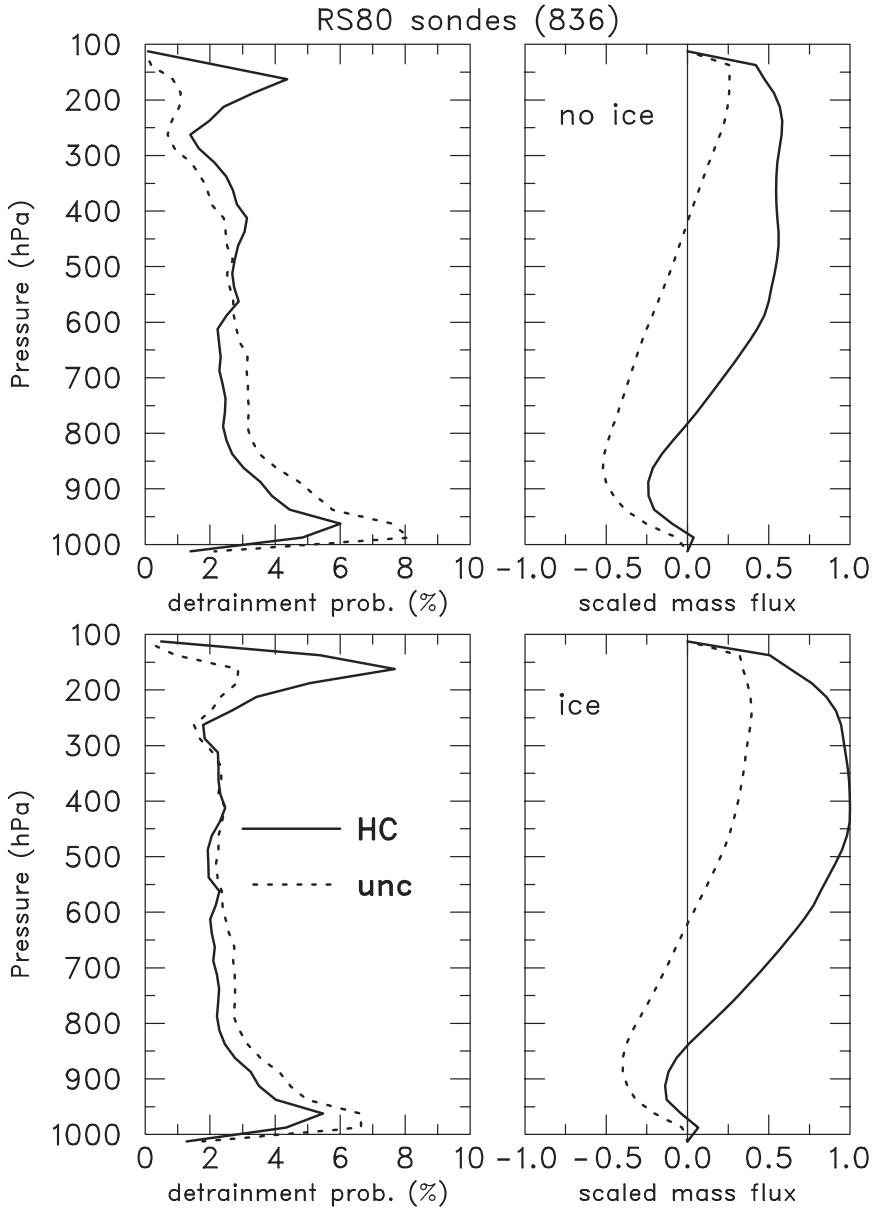

FIG. 17. Vertical profiles of (left) detrainment probability and (right) scaled convective mass flux from the Raymond–Blyth buoyancy-sorting cloud model computed with humidity-corrected (HC; solid line) and humidity-uncorrected (unc; dashed line) data for the RS80 sonde type. Results are shown with (top) no-ice effects and (bottom) where ice formation is allowed. All mass flux profiles have been normalized by the largest flux value, which in this case is the HC mass flux at 400 hPa in the bottom-right panel.

allowing more parcels to detrain at higher levels. These changes in detrainment resulting from the use of humidity-corrected data translate into a 72% increase in the convective mass flux near 500 hPa. The changes in the mass flux resulting from the humidity corrections at the other sites are listed in Table 5. As one might expect from the smaller corrections in the other sonde types, the mass flux increases resulting from the humidity corrections are substantially smaller at these other sites.

The analysis presented in this section suggests that simulated convection using the humidity-corrected sondes would occur with much greater intensity and frequency. Without the corrections, the dry low levels as depicted in the low CAPE and high CIN values of the RS80 sondes would inhibit deep convection in their vicinity. Also, the

TABLE 5. Mass flux increase near 500 hPa resulting from the use of humidity-corrected sondes in the cloud model. Only sondes with no missing data up to 100 hPa were used in this analysis (the number of these complete sondes for each sonde type is shown in the center column).

Sonde type	No. of sondes	Mass flux increase (%)
RS80	835	72
RS92	610	4
MEISEI	373	19
Graw (Laoag only)	65	18

spatial distribution of simulated convection should change considerably when using the humidity-corrected sondes because moistening associated with frontal boundaries will be more accurately depicted.

8. Summary and concluding remarks

The enhanced upper-air sonde network of TiMREX included 13 sites: 8 operational sites that increased their launch frequency, 3 additional land sites, and 2 research vessels. In addition, several dropsonde missions were conducted over the waters surrounding Taiwan. During its 42-day special observing period from 15 May through 25 June 2008, the TiMREX network had 2330 successful sonde launches. Part of the challenge of processing this upper-air dataset is that four different sonde types were used (RS80, RS92, MEISEI, and Graw). Postprocessing of the sonde data revealed a number of issues, including a significant dry bias at four of the sites using RS80 sondes and contaminated low-level thermodynamic data at one of the ships. This paper describes the corrections applied to these sondes and details the entire quality-control process, which includes assigning QC flags to suspect data (e.g., bad winds) that are identifiable but not correctable.

A variety of humidity corrections were applied to several of the sounding sites. These include use of corrected humidity coefficients developed at Vaisala for three of the RS80 sites. At the fourth RS80 sites (Hualien), a CDF matching scheme was used that is based on an intercomparison dataset collected at Pingdong during the experiment. This approach attempts to match the statistics of the questionable RS80 sondes to the more reliable RS92 sondes. A CDF matching scheme, based on intercomparison launches collected at Banchiao, was used to correct the MEISEI and Graw sondes as well. A correction, designed to remove the daytime dry bias resulting from solar heating of the humidity instrument, was applied to the RS80 and RS92 sondes as well as to the other sondes, which were corrected to the standard of the RS92.

While no obvious humidity biases were observed in the sonde data from the southern ship, more than 80% of the soundings had unrealistically large gradients of T and T_d in the lowest few hundred meters. Although the exact cause of these large gradients is unclear, it was likely related to contamination from the ship structure because these problems were exaggerated during the daylight hours when solar-heating effects would be most prominent. A simple correction scheme was devised to correct the contaminated data. In this procedure, computed gradients of good data were extrapolated to the surface. The procedure produced corrections at the surface on the order of 2°–3°C with an estimated error of 0.2°C or less. Without the correction, the SST $-$ T_s difference is generally negative (i.e., $T_s >$ SST), with a period mean of -0.63°C. With the correction, the difference shows a more reasonable difference of 0.94°C, similar to that observed in a previous experiment in this region.

The primary impacts of the corrections are as follows:

- At the RS80 sites, the SOP-mean RH increased about 10% ($\sim$2 g kg^{-1}) near the surface, decreasing to about $\sim$5% at upper levels. In the RS92 sondes, the RH correction is very small near the surface, increasing to about 20% at the upper levels. The consistency between the RS80- and RS92-corrected mean humidity profiles is much better, especially in the lower troposphere, where mean near-surface values are around 80% (or 17 g kg^{-1}).
- Comparison of sonde total column precipitable water with independent estimates (from ground-based GPS systems and satellites) shows that the corrections have reduced the dry bias in the RS80 sondes from values of 5–8 mm to less than 2 mm, or within the accuracy of the independent estimates. This comparison and other analyses suggest that a slight dry bias may still be present in the corrected RS80 sondes at Makung and Hualien as well as, in the daytime, corrected RS92 sondes at Tainan, Henchun, and Taichung. Overall, these favorable comparisons give us confidence that the corrections have significantly improved the description of the moisture field.
- The intercomparison study at Banchiao, which formed the basis for the correction of the MEISEI and Graw sondes, was less than optimal, being conducted in nonmonsoonal conditions. However, the study did show that, of the three sondes tested, only the RS92 sondes attained saturation in cloudy conditions. Application of the corrections in the MEISEI and Graw sondes increased the low-level RH by a few percent ($\sim$0.5 g kg^{-1}), leading to a higher frequency of saturated layers and improved comparisons of PW to

independent estimates. Because certain aspects of these corrected sondes (e.g., a slight overmoistening of low levels) seem less beneficial, both corrected and uncorrected versions of the dataset are made available to be utilized at the user's discretion.

- Use of RS80-corrected sondes increases mean CAPE by 484 J kg^{-1} (a threefold increase) and decreases |CIN| by 80 J kg^{-1}. The changes in the convective parameters in the other sonde types are considerably smaller, consistent with their smaller corrections.
- The use of a buoyancy-sorting cloud model shows that the humidity corrections in the RS80 sondes result in a convective mass flux increase of 72% at midlevels. The mass flux increase resulting from the correction in the other sonde types is more modest—around 20% for the MEISEI and Graw sondes and ~5% for the RS92 sondes.

Based on the comparison of several analyses with and without humidity corrections, we contend that the corrected dataset described herein has resulted in a much-improved description of the moisture distribution during TiMREX. These improvements should lead to more accurate diagnostics studies, better initializations of models, and a high-fidelity dataset useful for calibration and validation of independent datasets. With the high sampling frequency of upper-air soundings in both space and time during TiMREX, in conjunction with the large suite of other instrumentation (radars, profiler, gauges, etc.) deployed over southern Taiwan, these TiMREX datasets will be invaluable resources for advancing our knowledge of heavy rain events in monsoonal conditions. In addition, the characteristics of humidity data from the four sonde types examined in this study and their correction methods will be useful for understanding biases in the historical radiosonde humidity data in Taiwan and other regions, as well as for helping to homogenize the radiosonde climatological data to study long-term water vapor trends. To encourage use of the quality-controlled sonde dataset described herein, it has been made available on the Internet, along with detailed dataset documentation (available from the SoWMEX/TiMREX data field catalog online at http://sowmex.cwb.gov.tw/2008/SoxDataLogin.php).

Acknowledgments. This research has been supported by the National Science Foundation under Grants ATM-0500061 and AGS-0966758. We thank Kate Young for her help in using the ASPEN software to create the L2 dataset, Jing-Shan Hong for providing the ground-based GPS data, Chris Davis for his insightful comments and suggestions, Chi-Rong Chen and the Taiwanese Central Weather Bureau (CWB) for their travel support for the first author, and the countless students and staff from the many agencies and universities in Taiwan who painstakingly took the upper-air observations. We also thank the three anonymous reviewers for their valuable comments that led to changes that greatly improved this paper.

REFERENCES

Agusti-Panareda, A., A. Beljaars, C. Cardinali, I. Genkova, and C. Thorncroft, 2010: Impact of assimilating AMMA soundings on ECMWF analyses and forecasts. *Wea. Forecasting,* **25,** 1142–1160.

Bock, O., M.-N. Bouin, A. Walpersdorf, J. P. Lafore, S. Janicot, F. Guichard, and A. Agusti-Panareda, 2007: Comparison of ground-based GPS precipitable water vapour to independent observations and NWP model reanalyses over Africa. *Quart. J. Roy. Meteor. Soc.,* **133B,** 2011–2027, doi:10.1002/qj.185.

Cady-Pereira, K. E., M. W. Shepherd, D. D. Turner, E. J. Mlayer, S. A. Clough, and T. J. Wagner, 2008: Improved daytime column-integrated precipitable water vapor from Vaisala radiosonde humidity sensors. *J. Atmos. Oceanic Technol.,* **25,** 873–883.

Chen, G. T. J., 2004: Research on the phenomena of Meiyu during the past quarter century: An overview. *East Asian Monsoon,* C. P. Chang, Ed., Series for Meteorology of East Asia, Vol. 2, World Scientific, 357–403.

Ciesielski, P. E., and R. H. Johnson, 2009: Atmospheric mixed layers over the South China Sea during SCSMEX. *SOLA,* **5,** 29–32, doi:10.2151/sola.2009-008.

——, ——, P. T. Haertel, and J. Wang, 2003: Corrected TOGA COARE sounding humidity data: Impact on the diagnosed properties of convection and climate over the warm pool. *J. Climate,* **16,** 2370–2384.

——, ——, and J. Wang, 2009: Correction of humidity biases in Vaisala RS80-H sondes during NAME. *J. Atmos. Oceanic Technol.,* **26,** 1763–1780.

Crook, N. A., 1996: Sensitivity of moist convection forced by boundary layer processes to low-level thermodynamic fields. *Mon. Wea. Rev.,* **124,** 1757–1785.

Fairall, C. W., E. F. Bradley, D. P. Rodgers, J. B. Edson, and G. S. Young, 1996: Bulk parameterizations of air–sea fluxes for TOGA COARE. *J. Geophys. Res.,* **101,** 3747–3764.

Ferrier, B. S., and R. A. Houze Jr., 1989: One-dimensional time dependent modeling of GATE cumulonimbus convection. *J. Atmos. Sci.,* **46,** 330–351.

Guichard, F., D. Parsons, and E. Miller, 2000: Thermodynamic and radiative impact of the correction of sounding humidity bias in the tropics. *J. Climate,* **13,** 3611–3624.

Johnson, R. H., P. E. Ciesielski, and K. A. Hart, 1996: Tropical inversions near the 0°C level. *J. Atmos. Sci.,* **53,** 1838–1855.

Jou, B. J.-D., and W.-C. Lee, 2009: SoWMEX/TiMREX overview. Preprints, *Int. Conf. on MCS and High-Impact Weather/Climate in East Asia (ICMCS-VII),* Seoul, Korea, East Asian Weather Research Association, 1–9.

Loehrer, S. M., T. A. Edmands, and J. A. Moore, 1996: TOGA COARE upper-air sounding data archive: Development and quality control procedures. *Bull. Amer. Meteor. Soc.,* **77,** 2651–2671.

Lorenc, A., D. Barker, R. Bell, B. Macpherson, and A. Maycock, 1996: On the use of radiosonde humidity observations in midlatitude NWP. *Meteor. Atmos. Phys.,* **60,** 3–17.

Nakamura, H., H. Seko, and Y. Shoji, 2004: Dry biases of humidity measurements from the Vaisala RS80-A and Meisei RS2-91 radiosondes and from ground-based GPS. *J. Meteor. Soc. Japan,* **82,** 277–299.

Nuret, M., J.-P. Lafore, F. Guichard, J.-L. Redelsperger, O. Bock, A. Agusti-Panareda, and J.-B. N'Gamini, 2008: Correction of humidity bias for Vaisala RS80-A sondes during the AMMA 2006 observing period. *J. Atmos. Oceanic Technol.,* **25,** 2152–2158.

Nuss, W. A., and D. W. Titley, 1994: Use of multiquadric interpolation for meteorological objective analysis. *Mon. Wea. Rev.,* **122,** 1611–1631.

Raymond, D. J., and A. M. Blyth, 1992: Extensions of the stochastic mixing model to cumulonimbus clouds. *J. Atmos. Sci.,* **49,** 1968–1983.

Stull, R. B., 1988: *An Introduction to Boundary Layer Meteorology*. Kluwer Academic, 666 pp.

Vömel, H., and Coauthors, 2007: Radiation dry bias of the Vaisala RS92 humidity sensor. *J. Atmos. Oceanic Technol.,* **24,** 953–963.

Wang, J., 2005: Evaluation of the dropsonde humidity sensor using data from DYCOMS-II and IHOP_2002. *J. Atmos. Oceanic Technol.,* **22,** 247–257.

——, and L. Zhang, 2008: Systematic errors in global radiosonde precipitable water data from comparisons with ground-based GPS measurements. *J. Climate,* **21,** 2218–2238.

——, H. L. Cole, D. J. Carlson, E. R. Miller, K. Beierle, A. Paukkunen, and T. K. Laine, 2002: Corrections of humidity measurement errors from the Vaisala RS80 radiosonde—Application to TOGA COARE data. *J. Atmos. Oceanic Technol.,* **19,** 981–1002.

——, D. J. Carlson, D. B. Parsons, T. F. Hock, D. Lauritsen, H. L. Cole, K. Beierle, and N. Chamberlain, 2003: Performance of operational radiosonde humidity sensors in direct comparison with a chilled mirror dew-point hygrometer and its climate implications. *Geophys. Res. Lett.,* **30,** 1860, doi:10.1029/2003GL016985.

Wentz, F. J., 1997: A well-calibrated ocean algorithm for special sensor microwave imager. *J. Geophys. Res.,* **102,** 8703–8718.

Yoneyama, K., M. Fujita, N. Sato, M. Fujiwara, Y. Inai, and F. Hasebe, 2008: Correction for radiation dry bias found in RS92 radiosonde data during the MISMO field experiment. *SOLA,* **4,** 13–16, doi:10.2151/sola.2008-04.

Zuidema, P., 1998: The 600–800-mb minimum in tropical cloudiness observed during TOGA COARE. *J. Atmos. Sci.,* **55,** 2220–2228.